

AtomVision: A machine vision library for atomistic images

Kamal Choudhary^{1,2}, Ramya Gurunathan¹, Brian DeCost¹, and Adam Biacchi³

¹Material Measurement Laboratory, National Institute of Standards and Technology,
Gaithersburg, 20899, MD, USA

²Theiss Research, La Jolla, 92037, CA, USA

³Physical Measurement Laboratory, National Institute of Standards and Technology,
Gaithersburg, 20899, MD, USA

December 7, 2022

Abstract

Computer vision techniques have immense potential for materials design applications. In this work, we introduce an integrated and general-purpose AtomVision library that can be used to generate, curate scanning tunneling microscopy (STM) and scanning transmission electron microscopy (STEM) datasets and apply machine learning techniques. To demonstrate the applicability of this library, we 1) generate and curate an atomistic image dataset of about 10000 materials, 2) develop and compare convolutional and graph neural network models to classify the Bravais lattices, 3) develop fully convolutional neural network using U-Net architecture to pixelwise classify atom vs background, 4) use generative adversarial network for super-resolution, 5) curate a natural language processing based image dataset using open-access arXiv dataset, and 6) integrate the computational framework with experimental microscopy tools. AtomVision library is available at <https://github.com/usnistgov/atomvision>.

1 Introduction

Only a few experimental techniques allow a materials scientist to “see” the local atomic structure of a sample. Atomistic imaging techniques such as scanning tunneling microscopy (STM), atomic force microscopy (AFM), transmission electron microscopy (TEM) and their variants provide insights into the local atomic structure, defects and their dynamics, which are critically linked to the functionality and performance of the materials [1]. Due to rapid growth in computer-vision techniques [2, 3], its application to atomic scale image data is natural. These data can be obtained from experimental as well as computational methods and recently their usage has become widespread [4–20]. Nevertheless, an integrated library to capture, curate, generate datasets and apply data-analytics methods is still needed.

Such libraries can be useful for microscopy image tasks such as image classification [7, 21–23], pixelwise learning (e.g., semantic segmentation) [17, 24–30], object/entity recognition, localization, super-resolution [31–35] etc. The application of such libraries encompasses multiple science domains such as materials science, condensed matter physics, biology etc [5, 8, 36].

Computationally, there are several methods for simulating STM and scanning transmission electron microscopy (STEM) images. STM images can be computationally simulated using Bardeen [37], Tersoff-Hamman [38] and Chen [39] methods. STM images can be either constant height or constant current based. For standard high angle annular dark field (HAADF) STEM, methods such as convolution, Bloch wave and multislice approximations [40–43, 43, 44] can be used. The convolution approximation is one of the fastest ways to simulate STEM images. It is based on an incoherent linear image model that convolves the probe point-spread function with simple atomic potentials for the specimen and are usually used for thin films. Bloch wave and multislice methods are computationally heavy but are more generalizable.

Some of the major libraries (experimental and computational) based on microscopy images include ab initio Transmission Electron Microscopy (abTEM) [45], EXtraction, Separation, and Caption-based natural Language Annotation of IMages (EXCLAIM) [23], AtomAI [46], [47], Prismatic [48] and Quantitative TEM/STEM Simulations (QSTEM) [49]. Deep learning techniques such as convolutional neural network (CNN) are commonly applied to atomistic image data. There have been several previous works on the application of deep-learning (DL) techniques [5] to atomistic image data. In Ref [24] pixelwise DL was applied to detect atoms in simulated atomic-resolution TEM images of graphene. A neural network model was developed to detect the presence of atoms as well as predict its height. Ref [25] demonstrated atomistic defect recognition and tracking across sequences of atomic-resolution STEM images of WS₂. In ref [26] U-net architecture was used to detect vacancies and dopants in WSe₂ in STEM images with high model accuracy. In ref [27] DefectSegNet was developed to automatically identify defects in transmission and STEM images of steel including dislocations, precipitates, and voids. Ziatdinov *et al.* applied DL techniques to learn surface molecular structures [29]. More details about previous works on atomistic imaging and machine learning techniques can be found elsewhere [5, 8, 36].

In this work, we present the AtomVision library, which can be used to generate a simulated STM/STEM dataset using several levels of approximation, as well as using natural language processing to collect images from literature and experiments. We also provide generalized scripts that can be used for a broad level of image machine learning tasks such as identifying five 2D-Bravais lattices [50], atomistic segmentation to distinguish between background and images and later apply convolutional neural network (CNN)/graph neural network (GNN) on the segmented images, and generative design of atomistic images using generative adversarial network (GAN) techniques. This library is a part of the NIST-JARVIS (Joint Automated Repository for Various Integrated Simulations) infrastructure [51] for accelerated materials design using electronic structure, force-field, machine learning calculations and experiments. The atomvision library is publicly available at <https://github.com/usnistgov/atomvision>.

2 Methods

2.1 Dataset generation and curation

We use Tersoff-Hamann (TH) technique [38] to calculate the STM images of 2D materials. TH is a simple model of an s-wave STM tip.

$$n(r, E) = \sum_{\mu} |\psi(r)|^2 \delta(\epsilon_{\mu} - E) \quad (1)$$

$$\int_{E_F}^{E_F + eV} n(r, E) dE \quad (2)$$

In this approach, the tunneling current I , which depends on the tip position r and the applied voltage V , is proportional to the integrated local density of states (ILDOS). The ILDOS is calculated from the Kohn-sham eigenvectors, ψ_μ , and eigenvalues, ϵ_μ , where μ labels different states. E_F is the Fermi-energy. Different experiments will choose different applied voltages, but we concentrate on two values, 0.5 eV for positive bias and -0.5 eV for negative bias, which require integrating from E_F to $E_F \pm 0.5$ eV. We choose 0.5 eV range for simplicity sake, and other values usually produce qualitatively similar images for metals or small gap semiconductors. However, simulations for other voltages should also be possible with the method and tools discussed in this work. This method is readily available in DFT software such as Vienna ab initio simulation package (VASP) [52, 53].

The STEM images [40–43, 43, 44] were generated with the convolution approximation (based on fast Fourier transform based convolutions) following:

$$I(r) = R(r, Z) \otimes PSF(r) \quad (3)$$

where r is a 2D vector in the image plane, $I(r)$ is the image intensity,

$$R(r, Z) = \sum_i^N Z_i^{1.7} \delta(r - r_i) \quad (4)$$

$R(r, Z)$ is the transmission function of the N atoms at position r_i , and includes information about the atomic potential of the system given by Z_i , the atomic number of the atom. Rutherford scattering from the nuclear charge predicts a Z^2 dependence of the intensity, but the exponent is reduced by core electron screening, and depends on the detection collection angles. The power value of 1.7 is an approximate value that represents a compromise between these many factors. In previous works, the power values of 1.3–1.7 [54] have also been used to match experiments, however, for the sake of generality, we use 1.7 for all the systems. We note that for such STEM images only crystallographic coordinates and atom-type information are needed. The optimized geometry for the 2D materials were obtained from density functional theory calculations. We generate STEM images with output size of 256x256 pixels for at least 2.5 nm x 2.5 nm size. The microscope point spread function (PSF) is modeled as a normalized Gaussian with width of 0.5 Å. We use the 2D materials available in the JARVIS-DFT-2D [51, 55], Computational 2D Materials Database (C2DB) [56] and 2DMatPedia [57] datasets, leading to 9150 systems with unique chemical compositions and structural spacegroup information.

For natural language processing (NLP) related dataset, we use the open access arXiv dataset, which consists of 1.8 million articles starting from 1986 to 2020. We use ChemNLP [58] to extract chemistry information from the arXiv articles. We search for keywords such as STEM, STM, microscopy, HRTEM, scanning tunneling microscopy and scanning transmission electron microscopy in the abstract and figure captions of articles, and if the system has that info, we further find out if the article contains clear STM/STEM images to curate an image dataset. The figure caption parsing was carried out with the BeautifulSoup package.

Currently, the experimental STEM image dataset consists of images of nanoparticles. As an example experimental dataset we use TEM images of Iron oxide (Fe_3O_4), rhodium (Rh), and tin(II) sulfide (SnS) nanoparticles. In future, we plan to expand this dataset to multiple systems, especially for the materials available in the JARVIS-DFT dataset. Iron oxide, rhodium, and tin(II) sulfide nanostructures were synthesized using previously reported solution strategies based on the thermal decomposition of elemental precursors. All

syntheses were carried out under Ar using standard Schlenk techniques. Briefly, Fe_3O_4 spherical nanoparticles were synthesized by heating iron oleate in benzyl ether to 300 °C and then centrifugally washing twice before dispersing the collected product in hexanes [59]. Rh triangular nanoplates were synthesized by heating $\text{RhCl}_3 \cdot x\text{H}_2\text{O}$ and 40,000 molecular weight poly(vinylpyrrolidone) in triethylene glycol to 135 °C before then centrifugally washing twice and redispersing the product in ethanol [60]. α -SnS micron-sized nanoribbons were synthesized by heating SnCl_2 and sulfur powder in oleylamine to 180 °C and then centrifugally washing twice before redispersing the product in toluene [61]. Transmission electron microscopy (TEM) images were collected using a Phillips EM-400 operating at an accelerating voltage of 120 kV and high-resolution TEM (HRTEM) images were obtained with a FEI Titan 80-300 operating at 300 kV. Samples were prepared by casting one drop of dilute nanomaterial solution onto 300-mesh Formvar and carbon-coated copper grids (Ted Pella). Please note that commercial products used in this work are identified to specify procedures. Such identification does not imply recommendation by National Institute of Standards and Technology (NIST).

2.2 Machine learning model

For the machine learning models, we primarily use the STEM dataset developed with the convolution approximation. We use several machine/deep learning approaches such as clustering, classification with convolution and graph convolution neural network, fully convolutional neural network using U-Net and generative adversarial network [4–20].

For clustering analysis, we use t-distributed stochastic neighbor embedding (t-SNE), which is a statistical method for visualizing high-dimensional data in a two- or three-dimensional map. The t-SNE plot was generated with the help of Scikit-learn library [62]. The images were flattened into a python numpy array and then their dimensionality was reduced using nonlinear t-SNE for visualization purposes.

The pixelwise classification/semantic segmentation task was performed with segmentation-models-with-pytorch (SMP) [63] package using U-Net [64] pretrained model using Binary cross-entropy with logits loss (BCELogitLoss) function. All the supervised ML tasks used 75:25 training:testing of samples during training.

For the Bravais lattice classification task, we use DenseNet (Dense Convolutional Network) [65] with pre-trained model available in PyTorch [66]. We use a uniform size of 256x256 images for each material. We use Pytorch-Ignite library to setup the training run with Adam optimizer, 0.001 learning rate and negative log likelihood loss (NLLLoss) for 100 epochs.

After pixelwise classification, we convert the images into networkx and deep graph library graphs [67], which are then used along with atomistic line graph neural network (ALIGNN) [68] for image classification tasks as well. We use maximum, minimum and mean intensity of blobs in the images as the node features, while a 4 Å cutoff is used to generate neighborlist and generate bond-angles of different nodes. We use a batch size of 32, learning rate of 0.001, AdamW optimizer, negative log likelihood loss (NLLLoss) and 50 epochs for ALIGNN training. We used the original hyperparameters of the ALIGNN model as used in ref. [68].

We create a synthetic dataset of STEM images with low resolution (4 times lower resolution, i.e. 64x64 pixel images instead of 256x256) and high-resolution (as generated with convolution approximation) images and train a generative adversarial network (GAN) for image super-resolution (SR) using SR-GAN model [69]. In SR-GAN, we use the 4th layer of VGG19 (visual geometry group convolutional neural network that is 19 layers deep) [70] as feature-extractor. We use a perpetual loss function during SR-GAN training, which is a combination of both adversarial loss and content loss. We train the model for 50 epochs, learning rate of 0.00008 and Adam optimizer during training.

Next, we analyze the reconstruction of image capabilities using an autoencoder model with PyTorch. We take the 256x256 image, and use an auto-encoder of dimension 1120. The decoding part of the model reconstructs the image in 256x256 size. We train the models for 200 epochs, with mean squared loss function, Adam optimizer, and a learning rate of 0.001.

3 Results

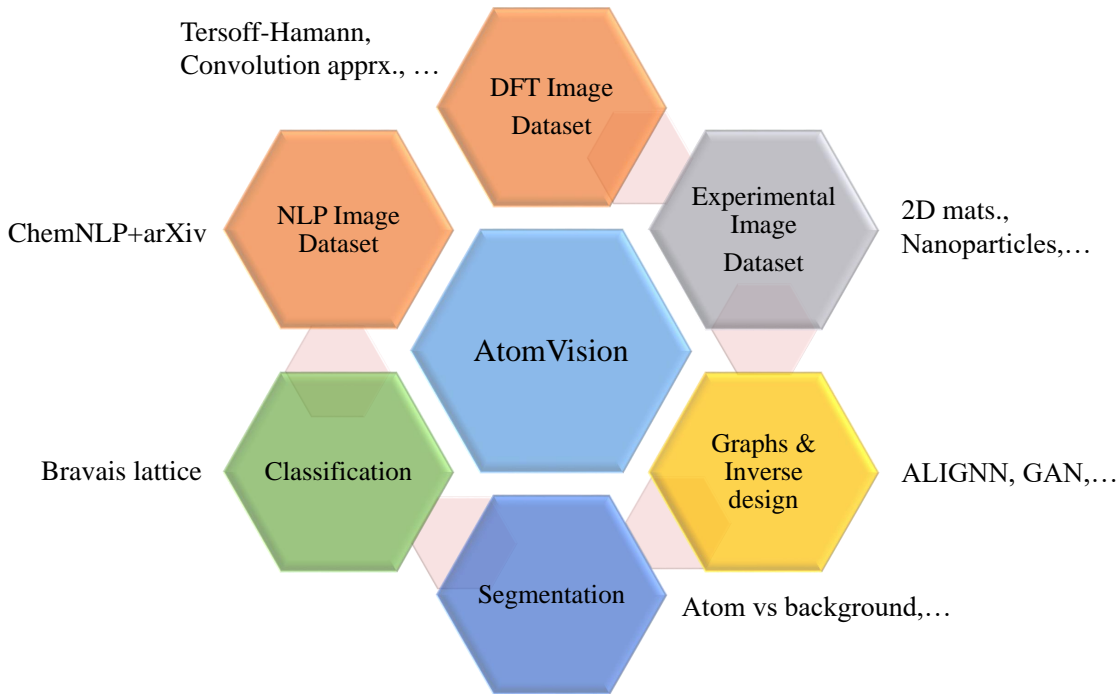


Figure 1: A Schematic overview of the AtomVision library. AtomVision presents an integrated library of dataset and AI/ML tools for atomistic images. The tool can be used for generating and curating microscopy dataset in a systematic manner as well as apply machine learning tools on the image dataset.

A schematic overview for AtomVision library is shown in Fig. 1. Usually any image analytic technique application would require a large dataset. In AtomVision, the dataset can be obtained from density functional theory, convolution approximation, natural language approximation, and experiments. For instance, STM images for 2D materials in both positive and negative biases were obtained from the Tersoff-Hamann approach as implemented in the JARVIS-Tools. The STM image consists of 1400 images for 2D materials in the JARVIS-DFT dataset. Although the application has been carried out for 2D materials, it can be applied to other non-2D systems as well. The STEM image dataset for 2D materials were obtained with the convolution approximation for systems in JARVIS-DFT, C2DB and 2DMatPedia computational datasets. While STM techniques require charge densities and wavefunctions to obtain integrated DOS values, the STEM dataset using the convolution approximation can be directly obtained with atomic types and coordinates information only.

We also show some of the machine learning architectures adopted in AtomVision in Fig. 2. These models are based on well-known deep learning models such as convolution neural network (CNN), graph neural network (GNN), and generative models such as auto-encoders (AE) and generative adversarial networks

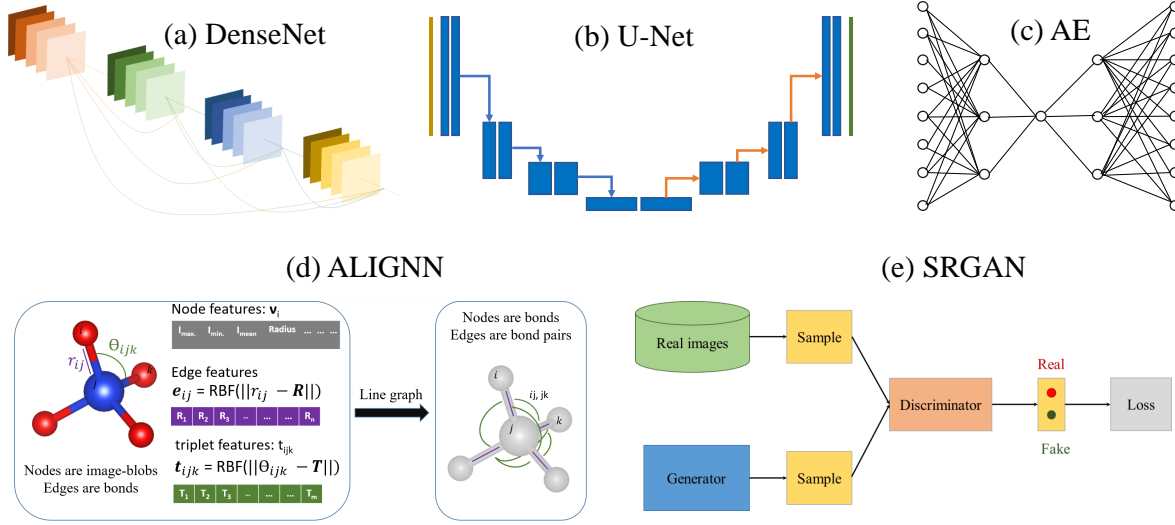


Figure 2: A few example machine learning architectures for images available in the AtomVision library. a) DenseNet is based on convolutional neural networks, b) U-net is a fully convolutional neural network, c) autoencoder, d) atomistic line graph neural network, e) super-resolution generative adversarial neural network.

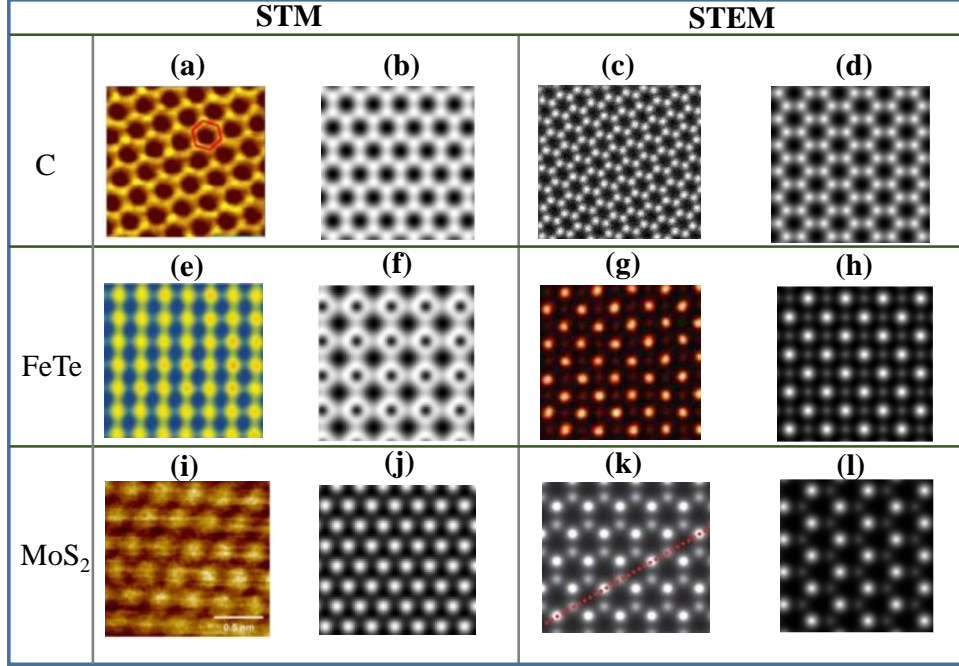
(GAN). The applications of these architectures and their performances are discussed in detail below.

3.1 Validation of dataset

We compare the STM and STEM simulated images of a few example 2D materials: graphene, FeTe and MoS₂, with experimental images in Fig. 3. The left panel (panels a,e,i) show experimental STM images, while DFT based images are shown in the next column (in panels b,f,j). Similarly, we show the experimental STEM images for graphene, FeTe, and MoS₂ in Fig. c,g,k and corresponding convolution approximation based images are shown in Fig. d,h,l. Clearly, we find excellent qualitative agreement between the simulated and experimental images. Furthermore, we note that theoretical image datasets are larger and can be generated in a very controlled way compares to experimental images. Hence, a comparison for a few samples gives a qualitative idea that computer vision techniques applied to a theoretical image dataset should indicate similar confidence with respect to experiments.

3.2 Clustering analysis

Next, we apply a machine learning clustering technique: t-SNE (t-distributed stochastic neighbor embedding) for visualizing the five types of 2D Bravais lattices in the JARVIS-DFT-2D STEM dataset. We first apply the t-SNE visualization directly to the simulated 256x256 pixel-based STEM image data for the 2D materials. These image array values for all the 2D materials in the datasets are converted into two-dimensions and are visualized in Fig. 4. From this visualization, it is clear that hexagonal class 0), square (class 1), and rectangle (class 2) systems segregate into islands in the pixel space, while the rhombus (class 3) and parallelogram



4

Figure 3: Comparison of our computational and previously reported experimental STM and STEM images for a few examples such as graphene, C (JVASP-667), FeTe (JVASP-6667), MoS₂ (JVASP-664). Fig. a,e,i shows experimental STM images [71–73] while b,f,j shows our simulated STM images. Similarly, c,g,k shows experimental [74–76] and d,h,l shows simulated STEM images. Experimental images are reprinted with permission from American Physical Society and American Institute of Physics Publishing.

(class 4) systems show greater overlap with other classes, suggesting more likely mis-classifications. We then perform a similar visualization using the graph-based features for the STEM image dataset. Here, the list of triplet graph features for each image, representing bond angle cosines, are encoded in a 200-bin histogram before applying the t-SNE operation to investigate clustering. Once again, we find noticeable clusters of the hexagonal and square systems, but noticeable overlap between the hexagonal and rhombus classes as well as the rectangle and parallelogram classes. Such analysis provides a visualization of large dimensional data in a compact way to suggest that both image pixel values and graph features contain information about the Bravais lattices.

3.3 U-Net and semantic segmentation

Although, the clustering models are useful for identifying global features of images such as lattice system, more details can be obtained with pixelwise classification of images. We use U-Net to perform atom vs background classification task using the STEM datasets. U-net is a fully convolutional neural network with a U-shaped architecture consisting of a specific encoder-decoder scheme (as shown in Fig. 2). The encoder reduces the spatial dimensions in every layer and increases the channels. On the other hand, the decoder increases the spatial dimensions while reducing the channels. We use the pretrained U-Net model in the SMP library and fine tune with the STEM dataset generated in this work for pixelwise classification of atom vs background classes. We find that high accuracy of 93.0 % for the pixelwise classification of atom vs background task. As an application for this model, we first generate synthetic graphene STEM images

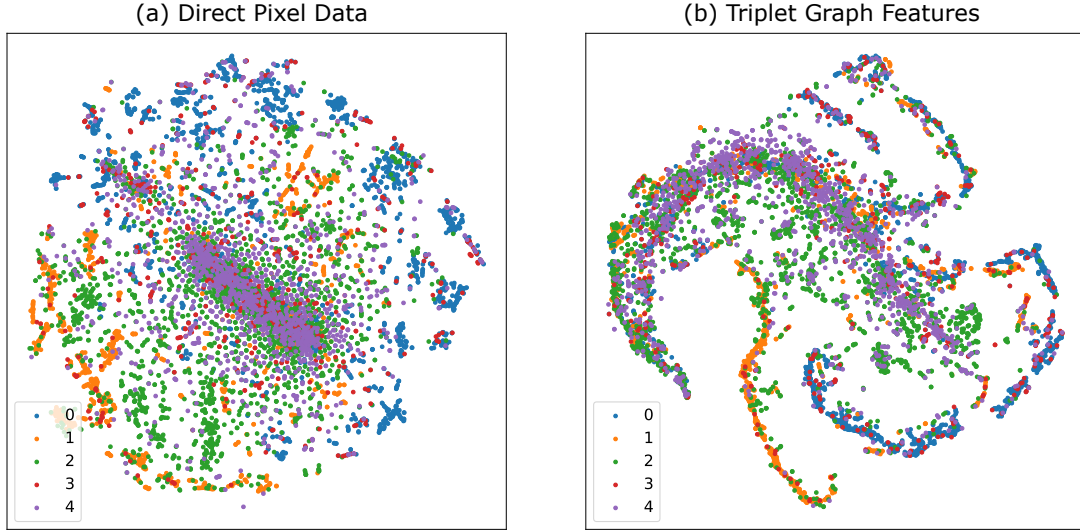


Figure 4: t-SNE visualization of the samples in the combined dataset including the JARVIS-DFT-2D and C2DB databases. In panel (a), the samples are featurized directly using the 256x256 pixel image intensity data. In contrast, in panel (b), the samples are featurized using their triplet (bond angle cosine) features in a graph construction. The distribution of triplet features are expressed as a 200-bin histogram ranging from -1 to 1. Here, we denote hexagonal, square, rectangle, rhombus and parallelogram classes as 0,1,2,3,4 respectively. We observe clusters of individual classes in both t-SNE figures.

with vacancies and use the semantic segmentation model on it as shown in Fig. 5. We find that the model can accurately identify atom and background from the image. Later, using scikit-image [77] based blob detection we can find the number of atoms in the image. With scikit-image, we can also get various statistics of the blobs such as the maximum, minimum, mean intensities in the blob etc.

3.4 CNN Classifier

Now, we use a supervised classification technique to classify images into the five 2D Bravais lattices: hexagonal, square, rectangular, rhombus (rectangular centered), and oblique (parallelogram) [50]. We use a well-known computer vision model: DenseNet to perform this task. In a DenseNet architecture, each layer is connected to every other layer, hence the name is given as Densely Connected Convolutional Network. For L layers, there are $L(L+1)/2$ direct connections. For each layer, the feature maps of all the preceding layers are used as inputs, and its own feature maps are used as input for each subsequent layers. DenseNet was developed to improve the vanishing gradient issues in deep convolutional neural networks. We fine-tune the DenseNet model [65] for 5 Bravais lattice classes using the STEM image dataset. We find that DenseNet provided an accuracy of 83.0 %. We note that the baseline model for such classification task in $1/5 = 20$ %, so using machine vision techniques is clearly justified. In addition to overall accuracy of the model, confusion matrix of the classification task provide details for individual class performance as shown in Fig. 6a. Here, we denote hexagonal, square, rectangle, rhombus and parallelogram classes as 0,1,2,3,4 respectively. We find that the trained model is highly accurate for hexagonal and square lattice but less accurate for rhombus and parallelogram classes, which can be attributed to less training data and higher complexity for these classes.

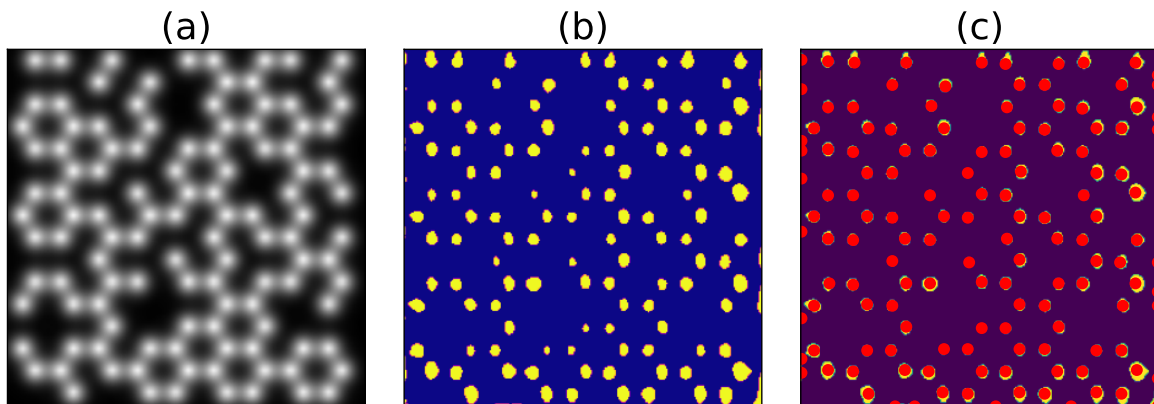


Figure 5: Application of semantic segmentation model to identify atoms and background from defective graphene system. In a) We generate synthetic graphene STEM images with vacancies and in b) use the semantic segmentation model. Finally, in c) we use a blob detection algorithm to find number of atoms.

3.5 ALIGNN-based GNN classifier

In the previous section, an image classifier was trained directly on the pixelated images. Here, we instead convert the image data into a non-Euclidean graph, which infers the connectivity of the objects in the image, allowing the usage of a graph neural network. Graph neural networks have been widely applied in the field of materials science as they allow for the structure of the material, along with composition-based features to be used in the prediction. Typically, graph neural networks are used to predict a material property from its structure, including both scalar quantities such as formation energy, bulk modulus, or band gap, or more recently, spectral quantities such as electron and phonon density-of-states or measured optical spectra (e.g. X-ray, infrared, Raman) [5]. To our knowledge, a graph neural network has not yet been applied to materials science image data, as it is in this work. The atomistic line graph neural network (ALIGNN) [68] was used, as it allows a hierarchy of structural features corresponding to single objects (i.e., atoms), pairs of objects (i.e., bond vectors), and pairs of bonds (i.e., bond angles). ALIGNN uses edge-gated graph convolution for updating nodes as well as edge features. One ALIGNN layer composes an edge-gated graph convolution on the bond graph with an edge-gated graph convolution on the line graph. The line graph convolution

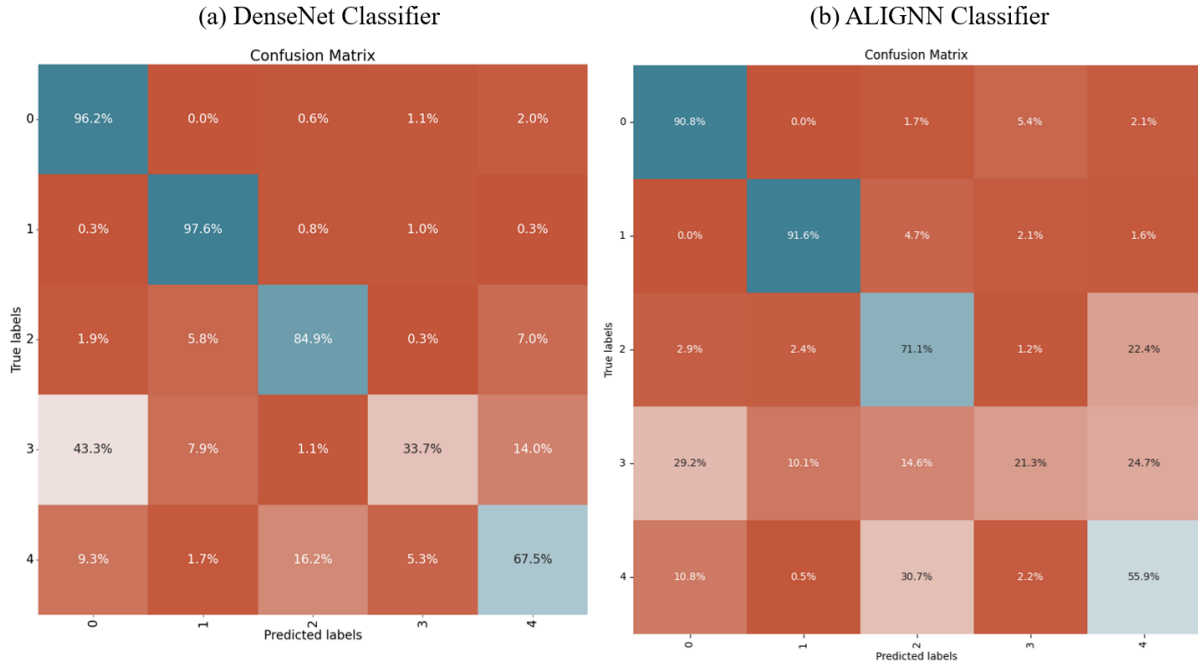


Figure 6: Confusion matrix for classifying STEM images into five Bravais lattices using a) convolution neural network based Densenet, b) graph neural network based ALIGNN models. Here, we denote hexagonal, square, rectangle, rhombus and parallelogram classes as 0,1,2,3,4 respectively.

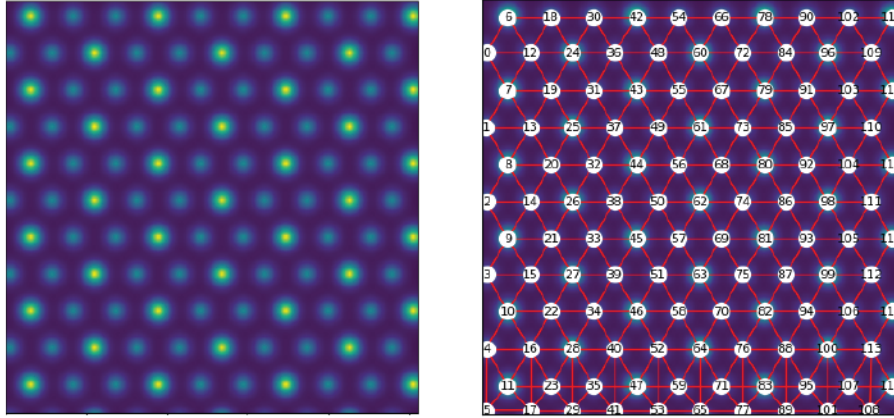
produces bond messages that are propagated to the atomistic graph, which further update the bond features in combination with atom features.

After the pixelwise classification, we can convert the data into graph that can capture non-Euclidean information of the images and can be used for advanced ML techniques such as the application of graph neural network. A example systems Pb_2I , GaTe and Nb_3Br_8 are shown in Fig. 7. After the graph conversion we use the ALIGNN model for lattice classification and find a reasonable accuracy of 78 %. Note that unlike the original ALIGNN model which uses atomic attributes such as electronegativity as node features, we use the blob-statistics (such as maximum, minimum and mean intensities in a blob) as the node attributes. Therefore, knowledge of chemistry is not required to train and execute the model. The confusion matrix for the model is shown in Fig. 6b. Although, the GNN-based models do not beat CNN models such as DenseNet, the framework for applying GNNs on images could be a powerful alternative tool for futuristic materials design because GNN-based methods can incorporate additional relationships and parameters that are not strictly related to the appearance of the image. Additionally, from Fig. 6, we find that both the CNN and GNN models work well for hexagonal and square lattice but they are less accurate for rhombus lattices.

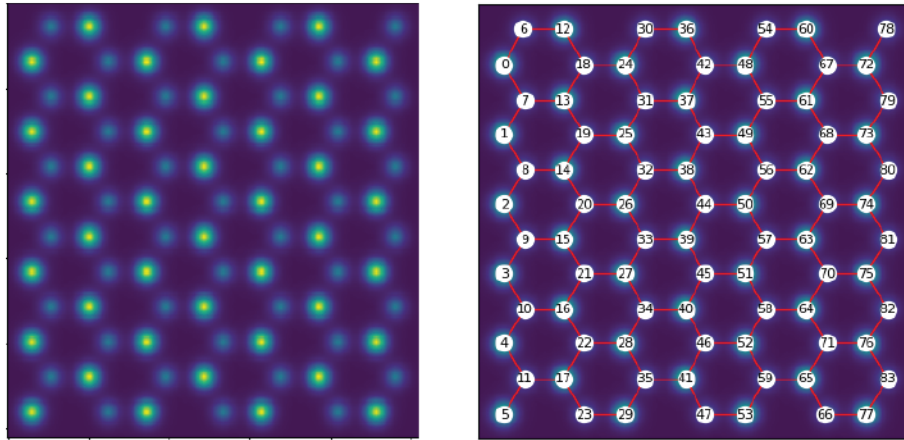
3.6 Autoencoders

Autoencoders (AE) are a special kind of neural network used to perform dimensionality reduction. We can think of autoencoders as being composed of two networks, an encoder and a decoder. The encoder learns a non-linear transformation from the original high-dimensional input space to a lower-dimensional latent space. A decoder learns a non-linear transformation that projects the latent vectors back into the original

PbI_2 : JVASP-76548



GaTe : JVASP-6838



Nb_3Br_8 : JVASP-76350

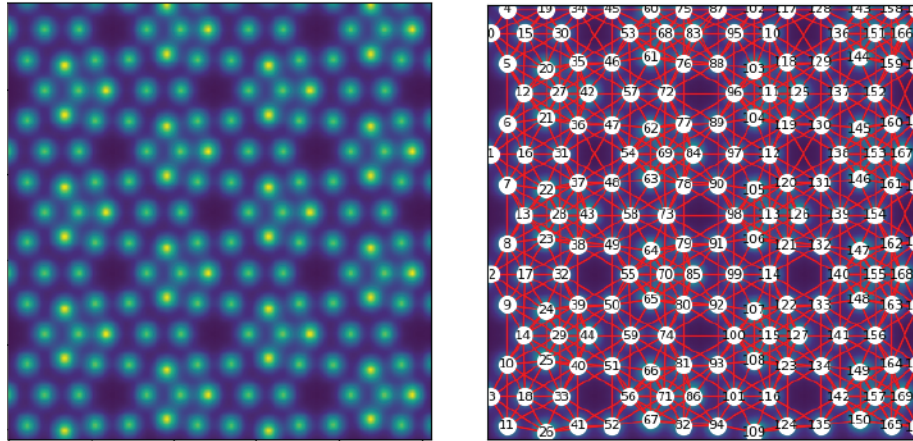


Figure 7: Computed STEM images (right) and overlaid graph construction (left) for three example materials in the hexagonal crystal system and (001) orientation. Although the lattices are visually diverse, the DenseNet and ALIGNN crystal system classifiers correctly categorize over 90 % of the class 0 samples.

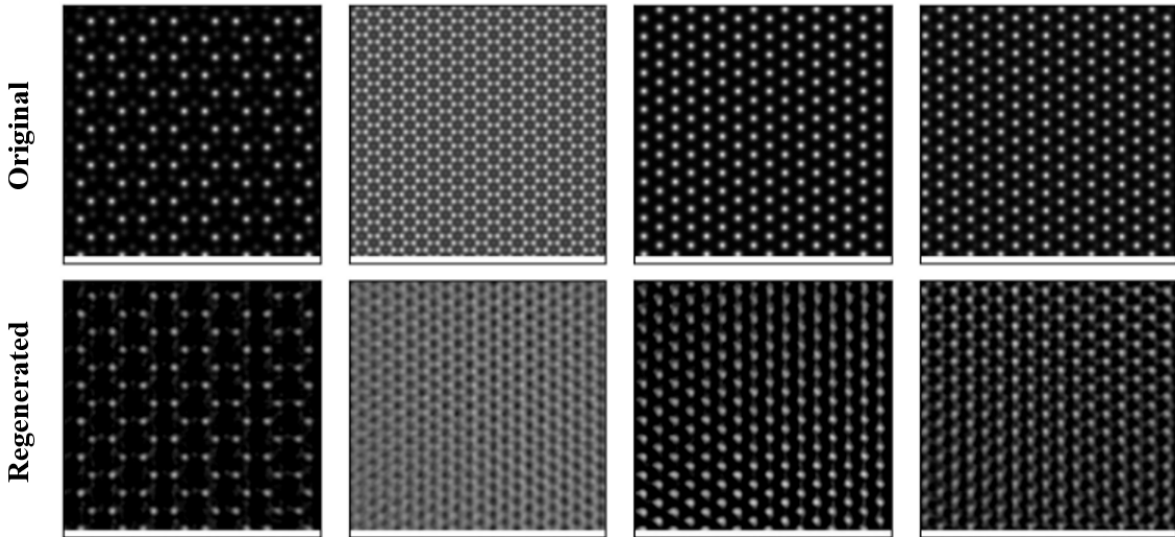


Figure 8: Original vs autoencoder regenerated images for a few random samples in the test dataset including Ti_2Se_3 , Al_2O_3 , ThF_2 , and CuF . The top 4 images are the original STEM images while the lower ones are generated after autoencoder regeneration operation.

high-dimensional input space. We develop an auto-encoder to reduce the large pixel-dimension. Usually an image taken as 256×256 if flattened leads to 50176 (i.e., 256×256) dimension, which is quite high. According to manifold hypothesis, the underlying structure of the data can be sufficiently described using only a few dimensions. Auto-encoders are well-known for such dimensional reduction tasks. We take the 256×256 image, and use an auto-encoder of dimension 1120. In Fig. 8, we show the performance of the auto-encoders to reconstruct a few images in the test dataset. Clearly, the reconstructed images bears a lot of similarity to the original images suggesting that the autoencoders developed in this work can be used for AE-related tasks such as dimensionality reduction.

3.7 Super-resolution GAN

Now, we use generative adversarial network (GAN) for enhancing the resolution of STEM images. We generate a dataset of 4-times low resolution (i.e., 64×64 instead of 256×256 size images) and using Super-Resolution Generative Adversarial Networks (SRGAN) [69] architecture, we develop a model to enhance resolution. We find a generator loss of 0.306 and discriminator loss of 0.458. Using this model, we generate a high-resolution image in the test set and show the results in Fig.9. The low-resolution image is shown as LR while the high-resolution image is shown as HR. SRGAN uses VGG19 (visual geometry group convolutional neural network that is 19 layers deep) [70] as feature extractor, however we notice that using shallow VGG19 feature extractor such as 4th layer (Fig. c) is equivalent to deeper layers such as Fig. d. Hence, a lower level feature extractor in VGG19 should be enough for resolution enhancement purposes.

3.8 Extracting images from arXiv dataset

Next, we use natural language processing with the open access arXiv dataset to curate datasets of STM and STEM images from the available literature. The arXiv dataset was previously used for ChemNLP project and has chemistry based information for the systems as well. We found more than 500 STM and 1500 STEM

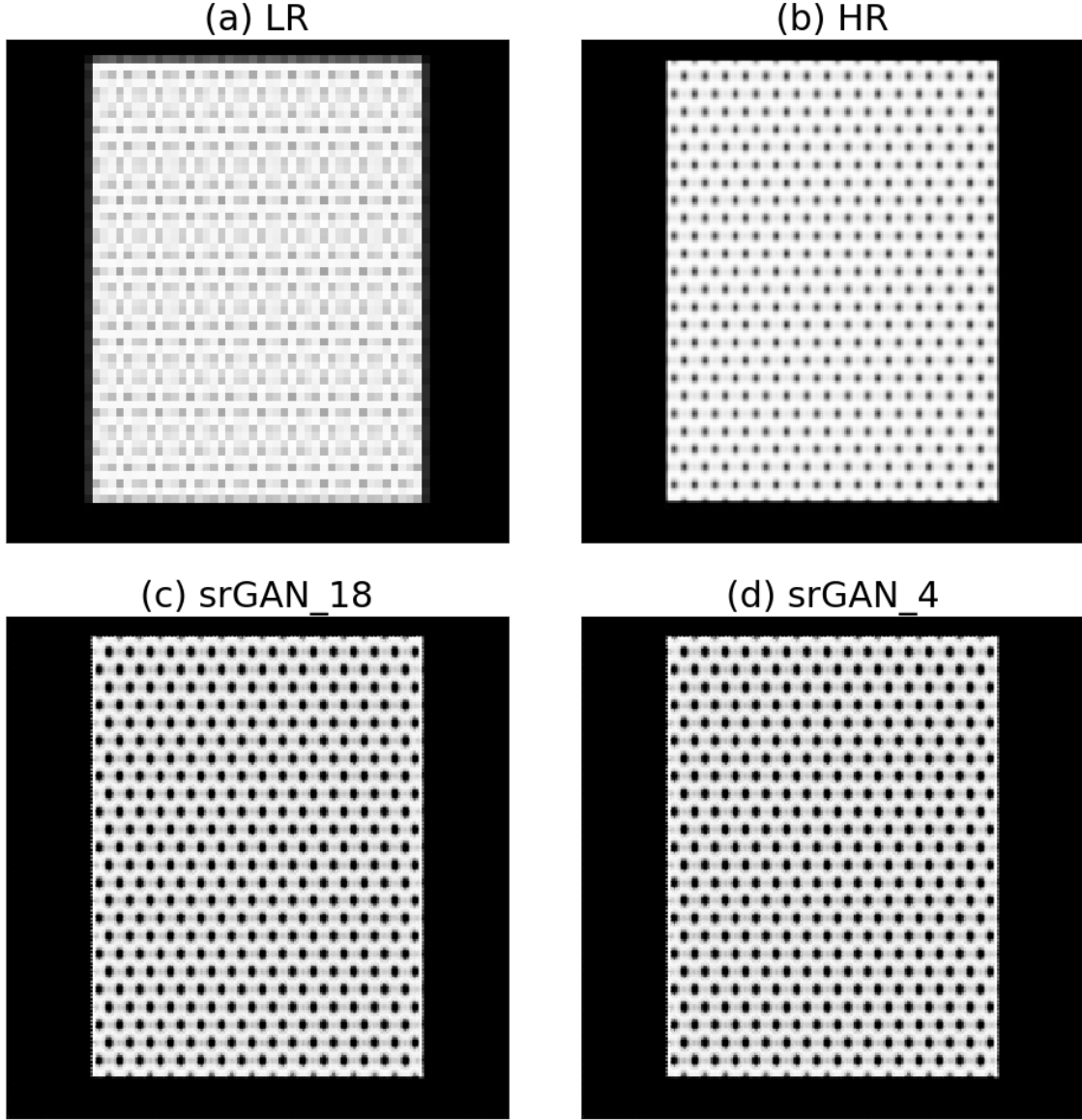


Figure 9: SR-GAN for enhancing image resolution. Examples for a) LR (low resolution), b) actual HR (high-resolution), c) SR-GAN VGG19’s 18th layer prediction, d) SR-GAN VGG19’s 4th layer prediction. We observe shallower layers of VGG19 gives similar predictions in terms of resolution enhancement as that of deeper layers.

images from a simple search of STM, STEM in abstracts for the condensed-matter physics articles in arXiv. We further searched for such entries in the figure captions of the dataset and found more than 1000 such images that can be useful for image analytics. We show a few of the images obtained from the arXiv dataset in Fig.10. We provide the list of links to the images and corresponding papers in the AtomVision library.

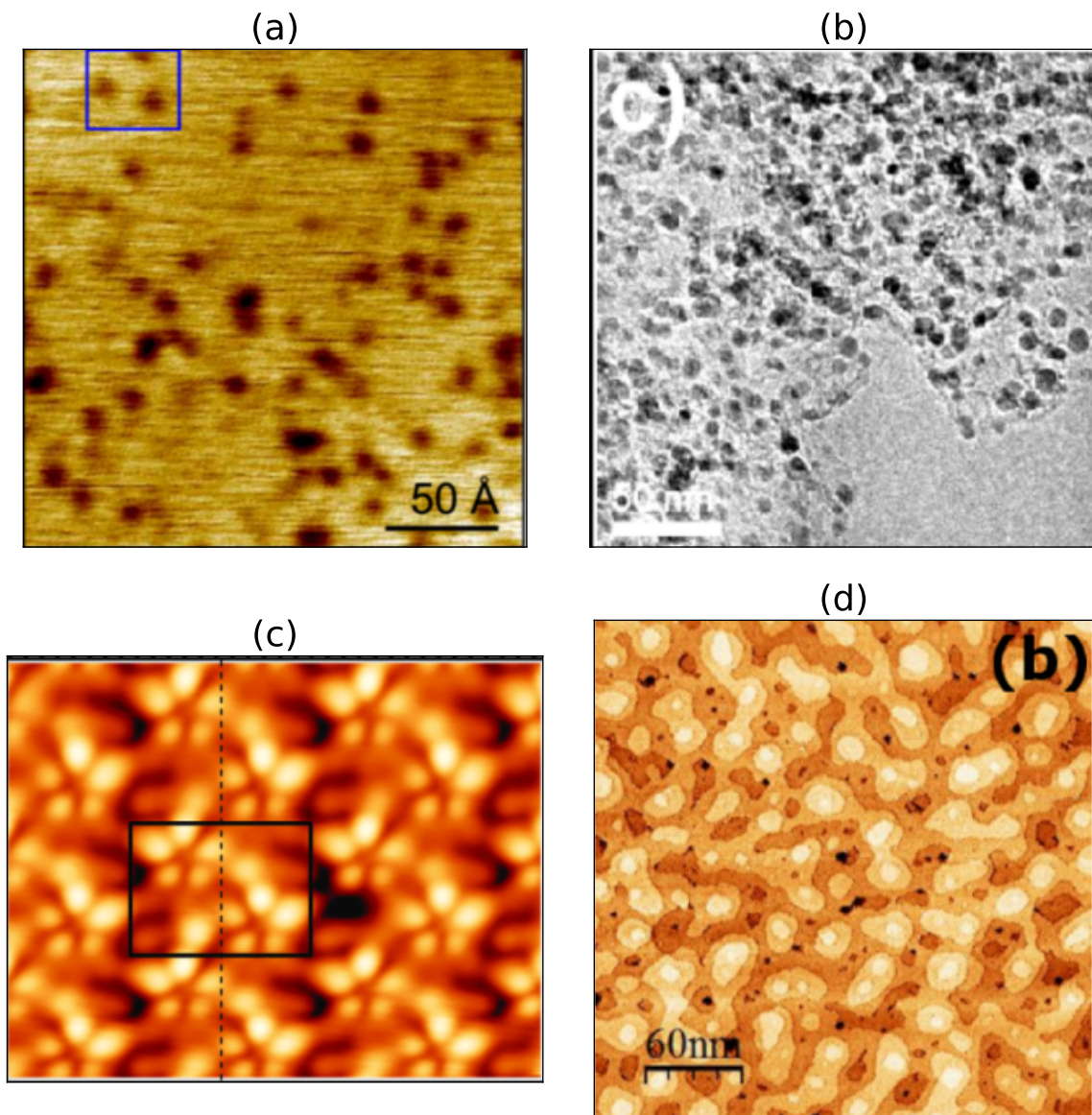


Figure 10: Example micrographs retrieved from the arXiv dataset. These figures are taken from: a) arXiv:0708.2306 for Dy [78], b) arXiv:0805.3416 for $\text{FeC}_{32}\text{H}_{16}\text{N}_8$ [79] c) arXiv:0807.3875 for Si [80] d) arXiv:0902.0626 for $\text{La}_{0.67}\text{Ca}_{0.33}\text{MnO}_3$ [81].

3.9 Experimental image dataset

In addition to computational and NLP based microscopy image datasets, we also develop our own experimental image dataset in AtomVision. AtomVision provides a flexible and easy to use metadata capture template that can capture experimental set up across various microscopy instruments. This is motivated by previous works in this field such as refs. [16, 82]. Such infrastructures provide frontend and backend meta-data capture schema and frameworks to capture and curate microscopy image data. Having an integrated framework for both experimental, computational and image based datasets in AtomVision will allow the investigation of several important challenges such as reproducibility, ground truth data and uncertainty in measurements.

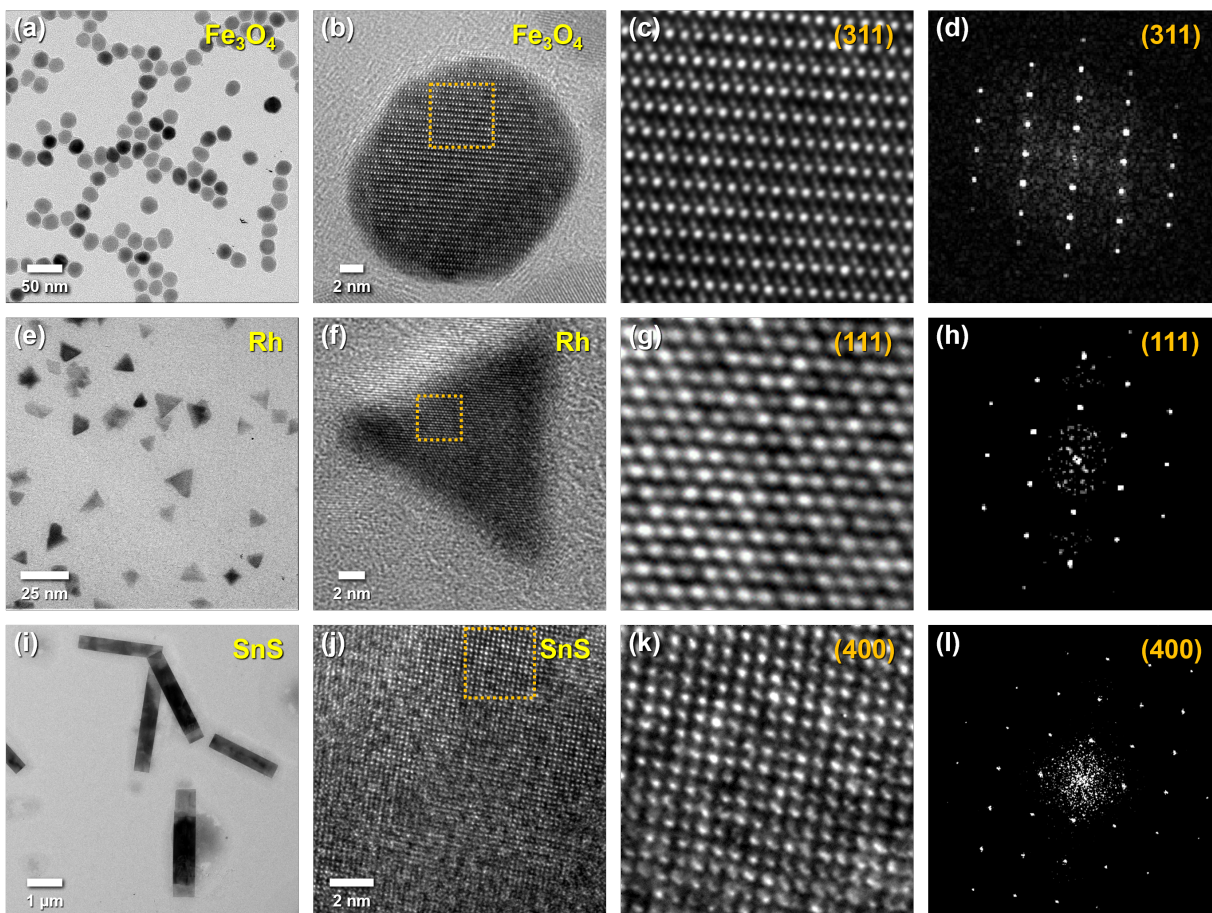


Figure 11: TEM and corresponding HRTEM images of solution-synthesized nanostructures. (a,b) Fe_3O_4 spherical nanoparticles, (e,f) Rh triangular nanoplates, and (i,j) SnS micron-sized nanoribbons. Regions of the HRTEM image indicated by dashed lines were magnified and analyzed by fast Fourier transform revealing crystallographic assignments of (c,d) Fe_3O_4 (311), (g,h) Rh (111), and α -SnS (400).

We show a few examples of TEM image dataset of nanoparticles in Fig.11. These nanoparticles TEM images are labelled by their different facet orientations leading to a huge variability in the dataset for the same material. Currently, the experimental image dataset contain a few hundreds of TEM images for various materials and their facets including Pt, Pd, Rh, Au, Fe_2O_3 , SnS etc. and we plan to continuously grow the dataset. We can integrate the AtomVision framework with NIST's and other microscopy measurement labs in the future to leverage several tools and datasets available in the library.

In summary, we have developed an integrated and general-purpose machine-vision library especially for atomistic images. The dataset in AtomVision consists of both computational, experimental and literature based images providing a wide variety for general applications including machine/deep learning applications. The dataset mainly consists of scanning tunneling microscopy (STM) and scanning transmission electron microscopy (STEM) images and the framework would allow other atomic image datasets as well. There are numerous image machine learning techniques and we demonstrated applications of few of them including convolution neural network, graph neural network, fully convolution neural network, generative adversarial network etc. Especially, the application of graph neural network such as ALIGNN on atomistic images provide a new paradigm for atomistic image analysis. The well-curated image dataset from experiments as

well as the computational images can serve as reference for many scientific applications.

4 Data availability statement

The data that support the findings of this study are openly available at the following URL: <https://github.com/usnistgov/atomvision>.

5 Acknowledgments

We thank the National Institute of Standards and Technology for funding, computational, and data-management resources. K.C. thanks the computational support from Extreme Science and Engineering Discovery Environment (XSEDE) computational resources under allocation number TG-DMR 190095. Contributions from K.C. were supported by the financial assistance award 70NANB19H117 from the U.S. Department of Commerce, National Institute of Standards and Technology.

References

- [1] Peter J Goodhew, John Humphreys, and Richard Beanland. Electron microscopy and analysis. CRC press, 2000.
- [2] Alex Krizhevsky, Ilya Sutskever, and Geoffrey E Hinton. Imagenet classification with deep convolutional neural networks. Communications of the ACM, 60(6):84–90, 2017.
- [3] Yaniv Taigman, Ming Yang, Marc’Aurelio Ranzato, and Lior Wolf. Deepface: Closing the gap to human-level performance in face verification. In Proceedings of the IEEE conference on computer vision and pattern recognition, pages 1701–1708, 2014.
- [4] Elizabeth A Holm, Ryan Cohn, Nan Gao, Andrew R Kitahara, Thomas P Matson, Bo Lei, and Srujana Rao Yarasi. Overview: Computer vision and machine learning for microstructural characterization and analysis. Metallurgical and Materials Transactions A, 51(12):5985–5999, 2020.
- [5] Kamal Choudhary, Brian DeCost, Chi Chen, Anubhav Jain, Francesca Tavazza, Ryan Cohn, Cheol Woo Park, Alok Choudhary, Ankit Agrawal, Simon JL Billinge, et al. Recent advances and applications of deep learning methods in materials science. npj Computational Materials, 8(1):1–26, 2022.
- [6] Rama K Vasudevan, Kamal Choudhary, Apurva Mehta, Ryan Smith, Gilad Kusne, Francesca Tavazza, Lukas Vlcek, Maxim Ziatdinov, Sergei V Kalinin, and Jason Hattrick-Simpers. Materials science in the artificial intelligence age: high-throughput library generation, machine learning, and a pathway from correlations to the underpinning physics. MRS communications, 9(3):821–838, 2019.
- [7] Mohammad Hadi Modarres, Rossella Aversa, Stefano Cozzini, Regina Ciancio, Angelo Leto, and Giuseppe Piero Brandino. Neural network for nanoscience scanning electron microscope image recognition. Scientific reports, 7(1):1–12, 2017.
- [8] Mengshu Ge, Fei Su, Zhicheng Zhao, and Dong Su. Deep learning analysis on microscopic imaging in materials science. Materials Today Nano, 11:100087, 2020.

- [9] Michiel Larmuseau, Michael Sluydts, Koenraad Theuwsen, Lode Duprez, Tom Dhaene, and Stefaan Cottenier. Compact representations of microstructure images using triplet networks. npj Computational Materials, 6(1):1–11, 2020.
- [10] Zijiang Yang, Xiaolin Li, L Catherine Brinson, Alok N Choudhary, Wei Chen, and Ankit Agrawal. Microstructural materials design via deep adversarial learning methodology. Journal of Mechanical Design, 140(11), 2018.
- [11] Tim Hsu, William K Epting, Hokon Kim, Harry W Abernathy, Gregory A Hackett, Anthony D Rollett, Paul A Salvador, and Elizabeth A Holm. Microstructure generation via generative adversarial network for heterogeneous, topologically complex 3d materials. JOM, 73(1):90–102, 2021.
- [12] Sehyun Chun, Sidhartha Roy, Yen Thi Nguyen, Joseph B Choi, HS Udaykumar, and Stephen S Baek. Deep learning for synthetic microstructure generation in a materials-by-design framework for heterogeneous energetic materials. Scientific reports, 10(1):1–15, 2020.
- [13] Minyi Dai, Mehmet F Demirel, Yingyu Liang, and Jia-Mian Hu. Graph neural networks for an accurate and interpretable prediction of the properties of polycrystalline materials. npj Computational Materials, 7(1):1–9, 2021.
- [14] Tiberiu Stan, Zachary T Thompson, and Peter W Voorhees. Optimizing convolutional neural networks to perform semantic segmentation on large materials imaging datasets: X-ray tomography and serial sectioning. Materials Characterization, 160:110119, 2020.
- [15] Ryan Cohn, Iver Anderson, Tim Prost, Jordan Tiarks, Emma White, and Elizabeth Holm. Instance segmentation for direct measurements of satellites in metal powders and automated microstructural characterization from image data. JOM, 73(7):2159–2172, 2021.
- [16] Joshua A Taillon, Thomas F Bina, Raymond L Plante, Marcus W Newrock, Gretchen R Greene, and June W Lau. Nexuslims: A laboratory information management system for shared-use electron microscopy facilities. Microscopy and Microanalysis, 27(3):511–527, 2021.
- [17] Brian L DeCost, Matthew D Hecht, Toby Francis, Bryan A Webler, Yoosuf N Picard, and Elizabeth A Holm. Uhcsdb: ultrahigh carbon steel micrograph database. Integrating Materials and Manufacturing Innovation, 6(2):197–205, 2017.
- [18] S Jesse, M Chi, A Belianinov, C Beekman, SV Kalinin, AY Borisevich, and AR Lupini. Big data analytics for scanning transmission electron microscopy ptychography. Scientific reports, 6(1):1–8, 2016.
- [19] Florian Schroff, Antonio Criminisi, and Andrew Zisserman. Harvesting image databases from the web. IEEE transactions on pattern analysis and machine intelligence, 33(4):754–766, 2010.
- [20] Xian-Sheng Hua and Jin Li. Prajna: Towards recognizing whatever you want from images without image labeling. In Twenty-Ninth AAAI Conference on Artificial Intelligence, 2015.
- [21] Angelo Ziletti, Devinder Kumar, Matthias Scheffler, and Luca M Ghiringhelli. Insightful classification of crystal structures using deep learning. Nature communications, 9(1):1–10, 2018.
- [22] Kamal Choudhary, Kevin F Garrity, Charles Camp, Sergei V Kalinin, Rama Vasudevan, Maxim Ziatdinov, and Francesca Tavazza. Computational scanning tunneling microscope image database. Scientific data, 8(1):1–9, 2021.

- [23] Eric Schwenker, Weixin Jiang, Trevor Spreadbury, Nicola Ferrier, Oliver Cossairt, and Maria KY Chan. Exsclaim!—an automated pipeline for the construction of labeled materials imaging datasets from literature. arXiv preprint arXiv:2103.10631, 2021.
- [24] Jacob Madsen, Pei Liu, Jens Kling, Jakob Birkedal Wagner, Thomas Willum Hansen, Ole Winther, and Jakob Schiøtz. A deep learning approach to identify local structures in atomic-resolution transmission electron microscopy images. Advanced Theory and Simulations, 1(8):1800037, 2018.
- [25] Artem Maksov, Ondrej Dyck, Kai Wang, Kai Xiao, David B Geohegan, Bobby G Sumpter, Rama K Vasudevan, Stephen Jesse, Sergei V Kalinin, and Maxim Ziatdinov. Deep learning analysis of defect and phase evolution during electron beam-induced transformations in ws2. npj Computational Materials, 5(1):1–8, 2019.
- [26] Sang-Hyeok Yang, Wooseon Choi, Byeong Wook Cho, Frederick Osei-Tutu Agyapong-Fordjour, Sehwan Park, Seok Joon Yun, Hyung-Jin Kim, Young-Kyu Han, Young Hee Lee, Ki Kang Kim, et al. Deep learning-assisted quantification of atomic dopants and defects in 2d materials. Advanced Science, 8(16):2101099, 2021.
- [27] Graham Roberts, Simon Y Haile, Rajat Sainju, Danny J Edwards, Brian Hutchinson, and Yuanyuan Zhu. Deep learning for semantic segmentation of defects in advanced stem images of steels. Scientific reports, 9(1):1–12, 2019.
- [28] Lukas Vlcek, Maxim Ziatdinov, Artem Maksov, Alexander Tselev, Arthur P Baddorf, Sergei V Kalinin, and Rama K Vasudevan. Learning from imperfections: predicting structure and thermodynamics from atomic imaging of fluctuations. ACS nano, 13(1):718–727, 2019.
- [29] Maxim Ziatdinov, Artem Maksov, and Sergei V Kalinin. Learning surface molecular structures via machine vision. npj Computational Materials, 3(1):1–9, 2017.
- [30] Oleg S Ovchinnikov, Andrew O’Hara, Stephen Jesse, Bethany M Hudak, Shi-Ze Yang, Andrew R Lupini, Matthew F Chisholm, Wu Zhou, Sergei V Kalinin, Albina Y Borisevich, et al. Detection of defects in atomic-resolution images of materials using cycle analysis. Advanced Structural and Chemical Imaging, 6(1):1–9, 2020.
- [31] Kevin de Haan, Zachary S Ballard, Yair Rivenson, Yichen Wu, and Aydogan Ozcan. Resolution enhancement in scanning electron microscopy using deep learning. Scientific reports, 9(1):1–7, 2019.
- [32] Jeffrey M Ede and Richard Beanland. Partial scanning transmission electron microscopy with deep learning. Scientific reports, 10(1):1–10, 2020.
- [33] Mohammad Rashidi and Robert A Wolkow. Autonomous scanning probe microscopy in situ tip conditioning through machine learning. Acs Nano, 12(6):5185–5189, 2018.
- [34] Sagi Eppel, Haoping Xu, Mor Bismuth, and Alan Aspuru-Guzik. Computer vision for recognition of materials and vessels in chemistry lab settings and the vector-labpics data set. ACS central science, 6(10):1743–1752, 2020.
- [35] Luke Scime, Derek Siddel, Seth Baird, and Vincent Paquit. Layer-wise anomaly detection and classification for powder bed additive manufacturing processes: A machine-agnostic algorithm for real-time pixel-wise semantic segmentation. Additive Manufacturing, 36:101453, 2020.

- [36] Ankit Agrawal and Alok Choudhary. Deep materials informatics: Applications of deep learning in materials science. Mrs Communications, 9(3):779–792, 2019.
- [37] John Bardeen. Tunnelling from a many-particle point of view. Physical review letters, 6(2):57, 1961.
- [38] Jerry Tersoff and Donald R Hamann. Theory and application for the scanning tunneling microscope. Physical review letters, 50(25):1998, 1983.
- [39] C Julian Chen and Walter F Smith. Introduction to scanning tunneling microscopy. American Journal of Physics, 62(6):573–574, 1994.
- [40] Aidan H Combs, Jason J Maldonis, Jie Feng, Zhongnan Xu, Paul M Voyles, and Dane Morgan. Fast approximate stem image simulations from a machine learning model. Advanced Structural and Chemical Imaging, 5(1):1–10, 2019.
- [41] Earl J Kirkland. Advanced computing in electron microscopy, volume 12. Springer, 1998.
- [42] Earl J Kirkland. Computation in electron microscopy. Acta Crystallographica Section A: Foundations and Advances, 72(1):1–27, 2016.
- [43] LJ Allen, SD Findlay, MP Oxley, and CJ Rossouw. Lattice-resolution contrast from a focused coherent electron probe. part i. Ultramicroscopy, 96(1):47–63, 2003.
- [44] JM Cowley and AF Moodie. Fourier images: I-the point source. Proceedings of the Physical Society. Section B, 70(5):486, 1957.
- [45] Jacob Madsen and Toma Susi. The abtem code: transmission electron microscopy from first principles. Open Research Europe, 1(24):24, 2021.
- [46] Maxim Ziatdinov, Ayana Ghosh, Tommy Wong, and Sergei V Kalinin. Atomai: a deep learning framework for analysis of image and spectroscopy data in (scanning) transmission electron microscopy and beyond. arXiv preprint arXiv:2105.07485, 2021.
- [47] Suhas Somnath, Chris R Smith, Stephen Jesse, and Nouamane Laanait. Pycroscopy-an open source approach to microscopy and microanalysis in the age of big data and open science. Microscopy and Microanalysis, 23(S1):224–225, 2017.
- [48] Colin Ophus. A fast image simulation algorithm for scanning transmission electron microscopy. Advanced structural and chemical imaging, 3(1):1–11, 2017.
- [49] Christoph Tobias Koch. Determination of core structure periodicity and point defect density along dislocations. Arizona State University, 2002.
- [50] Peter Moeck and P DeStefano. Accurate lattice parameters from 2d-periodic images for subsequent bravais lattice type assignments. Advanced Structural and Chemical Imaging, 4(1):1–33, 2018.
- [51] Kamal Choudhary, Kevin F Garrity, Andrew CE Reid, Brian DeCost, Adam J Biacchi, Angela R Hight Walker, Zachary Trautt, Jason Hattrick-Simpers, A Gilad Kusne, Andrea Centrone, et al. The joint automated repository for various integrated simulations (jarvis) for data-driven materials design. npj Computational Materials, 6(1):1–13, 2020.

- [52] Georg Kresse and Jürgen Furthmüller. Efficiency of ab-initio total energy calculations for metals and semiconductors using a plane-wave basis set. Computational materials science, 6(1):15–50, 1996.
- [53] Georg Kresse and Jürgen Furthmüller. Efficient iterative schemes for ab initio total-energy calculations using a plane-wave basis set. Phys. Rev. B, 54(16):11169, 1996.
- [54] Shunsuke Yamashita, Jun Kikkawa, Keiichi Yanagisawa, Takuro Nagai, Kazuo Ishizuka, and Koji Kimoto. Atomic number dependence of z contrast in scanning transmission electron microscopy. Scientific reports, 8(1):1–7, 2018.
- [55] Kamal Choudhary, Irina Kalish, Ryan Beams, and Francesca Tavazza. High-throughput identification and characterization of two-dimensional materials using density functional theory. Scientific Reports, 7(1):1–16, 2017.
- [56] Sten Hastrup, Mikkel Strange, Mohnish Pandey, Thorsten Deilmann, Per S Schmidt, Nicki F Hinsche, Morten N Gjerding, Daniele Torelli, Peter M Larsen, Anders C Riis-Jensen, et al. The computational 2d materials database: high-throughput modeling and discovery of atomically thin crystals. 2D Materials, 5(4):042002, 2018.
- [57] Jun Zhou, Lei Shen, Miguel Dias Costa, Kristin A Persson, Shyue Ping Ong, Patrick Huck, Yunhao Lu, Xiaoyang Ma, Yiming Chen, Hanmei Tang, et al. 2dmatpedia, an open computational database of two-dimensional materials from top-down and bottom-up approaches. Scientific data, 6(1):1–10, 2019.
- [58] Kamal Choudhary and Mathew L Kelley. Chemnlp: A natural language processing based library for materials chemistry text data. arXiv preprint arXiv:2209.08203, 2022.
- [59] Adam J Biacchi, Lucas M Johnson, Ashley B Sweet, Luke J Barrante, Eric M Cal, Angela R Hight Walker, and Matthew R Buck. Polyoxovanadates as precursors for the synthesis of colloidal multi-metal oxide nanocrystals. Chemistry of Materials, 34(7):2907–2918, 2022.
- [60] Adam J Biacchi and Raymond E Schaak. Ligand-induced fate of embryonic species in the shape-controlled synthesis of rhodium nanoparticles. ACS nano, 9(2):1707–1720, 2015.
- [61] Adam J Biacchi, Son T Le, Brian G Alberding, Joseph A Hagmann, Sujitra J Pookpanratana, Edwin J Heilweil, Curt A Richter, and Angela R Hight Walker. Contact and noncontact measurement of electronic transport in individual 2d sns colloidal semiconductor nanocrystals. ACS nano, 12(10):10045–10060, 2018.
- [62] Fabian Pedregosa, Gaël Varoquaux, Alexandre Gramfort, Vincent Michel, Bertrand Thirion, Olivier Grisel, Mathieu Blondel, Peter Prettenhofer, Ron Weiss, Vincent Dubourg, et al. Scikit-learn: Machine learning in python. the Journal of machine Learning research, 12:2825–2830, 2011.
- [63] Pavel Iakubovskii. Segmentation models pytorch. https://github.com/qubvel/segmentation_models.pytorch, 2019.
- [64] Olaf Ronneberger, Philipp Fischer, and Thomas Brox. U-net: Convolutional networks for biomedical image segmentation. In International Conference on Medical image computing and computer-assisted intervention, pages 234–241. Springer, 2015.

- [65] Gao Huang, Zhuang Liu, Laurens Van Der Maaten, and Kilian Q Weinberger. Densely connected convolutional networks. In Proceedings of the IEEE conference on computer vision and pattern recognition, pages 4700–4708, 2017.
- [66] Adam Paszke, Sam Gross, Francisco Massa, Adam Lerer, James Bradbury, Gregory Chanan, Trevor Killeen, Zeming Lin, Natalia Gimelshein, Luca Antiga, et al. Pytorch: An imperative style, high-performance deep learning library. Advances in neural information processing systems, 32, 2019.
- [67] Minjie Wang, Da Zheng, Zihao Ye, Quan Gan, Mufei Li, Xiang Song, Jinjing Zhou, Chao Ma, Lingfan Yu, Yu Gai, et al. Deep graph library: A graph-centric, highly-performant package for graph neural networks. arXiv preprint arXiv:1909.01315, 2019.
- [68] Kamal Choudhary and Brian DeCost. Atomistic line graph neural network for improved materials property predictions. npj Computational Materials, 7(1):1–8, 2021.
- [69] Christian Ledig, Lucas Theis, Ferenc Huszár, Jose Caballero, Andrew Cunningham, Alejandro Acosta, Andrew Aitken, Alykhan Tejani, Johannes Totz, Zehan Wang, et al. Photo-realistic single image super-resolution using a generative adversarial network. In Proceedings of the IEEE conference on computer vision and pattern recognition, pages 4681–4690, 2017.
- [70] Karen Simonyan and Andrew Zisserman. Very deep convolutional networks for large-scale image recognition. arXiv preprint arXiv:1409.1556, 2014.
- [71] Guohong Li, Adina Luican, and Eva Y Andrei. Scanning tunneling spectroscopy of graphene on graphite. Physical review letters, 102(17):176804, 2009.
- [72] Adam Mills, Yifei Yu, Chuanhui Chen, Bevin Huang, Linyou Cao, and Chenggang Tao. Ripples near edge terminals in mos2 few layers and pyramid nanostructures. Applied Physics Letters, 108(8):081601, 2016.
- [73] Can-Li Song, Yi-Lin Wang, Peng Cheng, Ye-Ping Jiang, Wei Li, Tong Zhang, Zhi Li, Ke He, Lili Wang, Jin-Feng Jia, et al. Direct observation of nodes and twofold symmetry in fese superconductor. Science, 332(6036):1410–1413, 2011.
- [74] Colum M O’Leary, Benedikt Haas, Christoph T Koch, Peter D Nellist, and Lewys Jones. Increasing spatial fidelity and snr of 4d-stem using multi-frame data fusion. Microscopy and Microanalysis, 28(4):1417–1427, 2022.
- [75] Lixing Kang, Chen Ye, Xiaoxu Zhao, Xieyu Zhou, Junxiong Hu, Qiao Li, Dan Liu, Chandreyee Manas Das, Jiefu Yang, Dianyi Hu, et al. Phase-controllable growth of ultrathin 2d magnetic fete crystals. Nature communications, 11(1):1–9, 2020.
- [76] Guilherme Migliato Marega, Yanfei Zhao, Ahmet Avsar, Zhenyu Wang, Mukesh Tripathi, Aleksandra Radenovic, and Andras Kis. Logic-in-memory based on an atomically thin semiconductor. Nature, 587(7832):72–77, 2020.
- [77] Stefan Van der Walt, Johannes L Schönberger, Juan Nunez-Iglesias, François Boulogne, Joshua D Warner, Neil Yager, Emmanuelle Gouillart, and Tony Yu. scikit-image: image processing in python. PeerJ, 2:e453, 2014.

- [78] D Wegner, A Bauer, and G Kaindl. Effect of impurities on tamm-like lanthanide-metal surface states. Physical Review B, 76(11):113410, 2007.
- [79] Christian Klinke and Klaus Kern. Iron nanoparticle formation in a metal–organic matrix: from ripening to gluttony. Nanotechnology, 18(21):215601, 2007.
- [80] Corsin Battaglia, Katalin Gaal-Nagy, Claude Monney, Clement Didiot, Eike Fabian Schwier, Michael Gunnar Garnier, Giovanni Onida, and Philipp Aebi. A new structural model for the si (331)-(12x1) reconstruction. arXiv preprint arXiv:0807.3875, 2008.
- [81] S Kelly, F Galli, I Komissarov, and J Aarts. Correlations between the morphology and the electronic structure at the surface of thin film manganites, investigated with stm. arXiv preprint arXiv:0902.0626, 2009.
- [82] Phuong Nguyen, Steven Konstanty, Todd Nicholson, Thomas O’Brien, Aaron Schwartz-Duval, Timothy Spila, Klara Nahrstedt, Roy H Campbell, Indranil Gupta, Michael Chan, et al. 4ceed: Real-time data acquisition and analysis framework for material-related cyber-physical environments. In 2017 17th IEEE/ACM International Symposium on Cluster, Cloud and Grid Computing (CCGRID), pages 11–20. IEEE, 2017.